A novel model for porous scaffold to match the mechanical anisotropy and the hierarchical structure of bone

Shiping Huang [a], Zhou Chen [a], Nicola Pugno [b,c], Qiang Chen [d,*], Weifeng Wang [a,**]

[a] School of Civil Engineering and Transportation, South China University of Technology, Wushan Road #381, Guangzhou 510640, PR China
[b] Department of Civil, Environmental and Mechanical Engineering, Università di Trento, Via Mesiano 77, 38123 Trento, Italy
[c] School of Engineering and Materials Science, Queen Mary University of London, Mile End Road, London E1 4NS, UK
[d] Biomechanics Laboratory, School of Biological Science and Medical Engineering, Southeast University, Nanjing 210096, PR China

ARTICLE INFO

ABSTRACT

A novel porous anisotropic scaffold with hierarchy is proposed for bone regeneration. The scaffold can mimic the morphology and the mechanical anisotropy of the natural bone. In this letter, the pores within the scaffold are prolate spheroidal and the structural anisotropy is controlled by the parameter β, which denotes the ratio of the semi-major axis to the semi-minor axis of the prolate spheroidal pores. The elastic-plastic behavior of the scaffold is studied for different porosities and β values using the finite element method. It has been found that the mechanical anisotropy depends on the parameter β, where a larger β leads to higher mechanical anisotropy. The scaffold's structure is simple and can be achieved easily in manufacturing with controllable porosity and anisotropy. Thus, the scaffold is a promising candidate for bone regeneration.

© 2014 Elsevier B.V. All rights reserved.

1. Introduction

Scaffolds play an important role in tissue regeneration since they provide temporary mechanical support within the defect. The ideal scaffold used for bone regeneration should possess mechanical properties that can match the bone properties [1]. The mechanical properties of bone are related to its hierarchical structure [2]. Therefore, porous scaffolds with hierarchical structure have been proposed to mimic the mechanical behavior of bone [3].

Numerous progresses have been made in the last two decades with respect to the scaffold materials, fabrication techniques and applications [1,4]. According to the experimental results using imaging technology [5], bone exhibits an anisotropic nature both in the extracellular bone matrix and in the morphology of the intertrabecular pores [6,7]. Correspondingly, the quantitative analysis of the mechanical behavior has been carried out by micromechanics [8–10] and finite element analysis (FEA) [5,11,12]. FEA is an effective approach to study stress/strain distributions of the scaffold and can also be used to develop poromechanics parameters [13], which influence the transport of pore fluid, hence

nutrients, and the mechanobiology of tissue regeneration and growth. One of the challenges in the scaffold design is to determine a continuum-level material model for the scaffold which can mimic the morphology and the mechanical behavior of the natural bone. In our previous work, we proposed a porous hierarchical scaffold [14,15], whose mechanical properties close to the natural bone could be tailored. However, the previous scaffold model could not simulate the structural and the mechanical anisotropy of the bone.

We have, therefore, proposed a novel porous anisotropic hierarchical scaffold. The elastic–plastic behavior of the scaffold is studied using FEA. The mechanical properties and the relationship between the structural and the mechanical anisotropy of the scaffold are investigated for different porosities.

2. Anisotropic model of the scaffold

To model the anisotropic morphology, the spherical pores used in our previous work [14,15] are replaced with the prolate spheroidal pores. The geometry of the one-level unit cell is represented by a cube (side length $2a^{(1)}$) from which a prolate spheroid with the same centroid, is excised, as seen in Fig. 1(a). The prolate spheroid is described as $x^2/(e^{(1)})^2 + y^2/(e^{(1)})^2 + z^2/(\beta e^{(1)})^2 = 1$, where $e^{(1)}$ is the semi-minor axis, $\beta e^{(1)}$ is the semi-major axis, and $\beta(>1)$ is the ratio of the semi-major axis
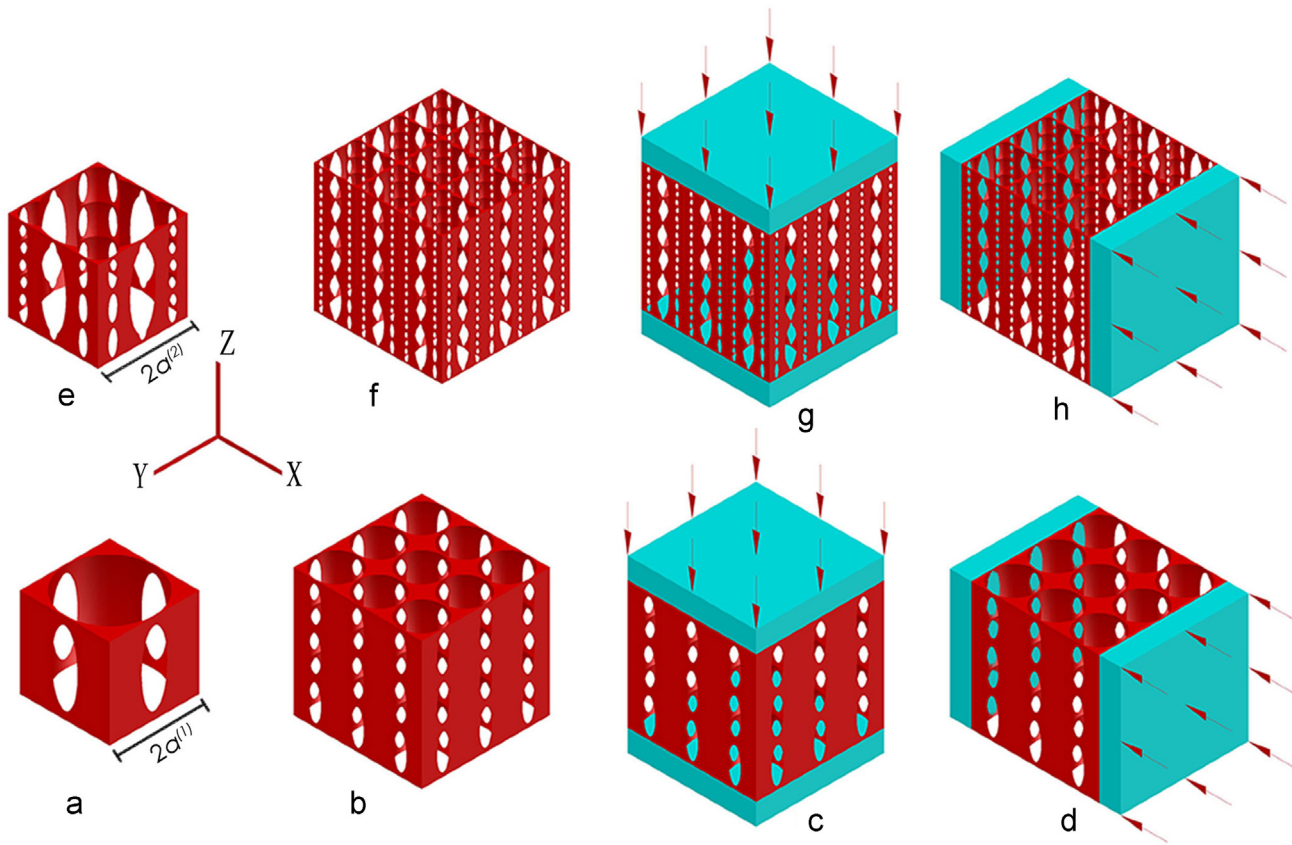
Fig. 1. Schematic of the porous anisotropic scaffold with hierarchy: (a) One-level unit cell; (b) one-level structure; (e) two-level unit cell; (f) two-level structure; (c), (d), (g) and (h) uniaxial loading in *Z*- and *X*-directions for one-level and two-level structure.

to the semi-minor axis. The two-level unit cell is composed of $n \times n \times n$ one-level unit cells (side length $2a^{(2)}=n \times 2a^{(1)}$), from which a prolate spheroid (semi-minor axis $e^{(2)}$ and semi-major axis $\beta e^{(2)}$) with the same centroid (Fig. 1(e)), is excised. The process is repeated for the higher level unit cell. For the *k*-level unit cell, it is noted that $a^{(k)}$ and $e^{(k)}$ must meet the condition $1 < e^{(k)}/a^{(k)} < \sqrt{\beta^2+1}/\beta$ in order to form interconnecting pores for cellular activity. The overall area of the *k*-level unit cell is $A^{(k)} = 4(a^{(k)})^2$. The one-level unit cell porosity calculated as $p^{(1)} = V_p^{(1)}/V_u^{(1)}$, where $V_p^{(1)}$ and $V_u^{(1)}$ are the pore volume and the unit cell volume, respectively. Through the simple geometric operation, the pore volume $V_p^{(1)}$ can be expressed as $V_p^{(1)}$ can be expressed as $p^{(1)} = \frac{4}{3}\pi\beta(e^{(1)})^3 - \pi(e^{(1)})^2(4\beta e^{(1)} - 4\beta a^{(1)} - 2a^{(1)} + 4\beta^3(a^{(1)})^3 + 2(a^{(1)})^3/3\beta^2 (e^{(1)})^2)$. Subsequently, the porosity of the *k*-level self-similar structure can be approximately expressed as $p^{(k)} = 1-(1-p^{(1)})^k$. It is noted that the porosity range decreases as β increases for the *k*-level scaffold, which is demonstrated in Fig. 2(a) and (b) for one-level and two-level scaffolds, respectively. Particularly, for the one-level and two-level unit cells with $\beta=1$, the porosity $p^{(1)}$ and $p^{(2)}$ are in the ranges of 52.4% to 96.5% and 75.5% to 99.7%, respectively, as seen in Fig. 2.

Many tissue-engineering base materials are commercially available for the scaffold [4,16]. As for scaffold manufacturing, non-designed controlled scaffold manufacturing method and designed controlled scaffold manufacturing method are used recently [1]. The latter method, such as nozzle deposition techniques, laser polymerization techniques, laser sintering techniques and printing techniques, is able to make complicated external anatomic shapes and complex internal porous architectures and thus can be used for our proposed scaffold

model. For illustrative purposes, we take the mechanical parameters of cortical bone for the constituent material used for the scaffold. The cortical bone can be simplified to be rate-independent elastic perfectly plastic material at extremely low loading rates [17]. To obtain the mechanical behavior of the proposed scaffold, a uniaxially loaded cube of the scaffold is studied using FEA, where the boundary conditions are shown in Fig. 1(c, d, g and h). Under the uniaxial loads, either compressive stress or tensile stress is dominant. Thus, we use the perfectly plastic von Mises model to simulate the scaffold's elastic–plastic response. However, under complex loads, since the tensile yield strength and compressive yield strength are different, some other failure criterions [18,19] have been proposed to account for it. To get the *k*-level structure's response, a uniform displacement Δ is applied on the surface until the structure fails and the corresponding reaction force $F^{(k)}$ is obtained at the same time, as shown in Fig. 1(c, d, g and h). For the *k*-level unit cell, the structure's Young's modulus and stress are calculated by $E^{(k)} = F/(2a^{(k)}\Delta)$ and $\sigma^{(k)} = F^{(k)}/A^{(k)}$, respectively. The structure's strength is obtained by $\sigma_y^{(k)} = F_y^{(k)}/A^{(k)}$, where $F_y^{(k)}$ is the reaction force at the point of structure's yielding. It is noted that the strain is obtained by $\varepsilon^{(k)} = \Delta/2a^{(k)}$.

In the FEA, the one-level model is formed by $3 \times 3 \times 3$ one-level unit cells, while the two-level model is formed by $3 \times 3 \times 3$ two-level unit cells, as seen in Fig. 1(c, d, g and h). The basic mechanical constants of the bovine cortical bone used here are $E_s = 15$ GPa, $\sigma_s = 225$ MPa and $\upsilon_s = 0.3$ [15], where E_s is the Young's modulus, σ_s is the yield stress in uniaxial loading test, and υ_s is Poisson's ratio.

3. Results and discussion

To demonstrate the mechanical anisotropy of the proposed model, we designed uniaxial loading tests for both of the one-level
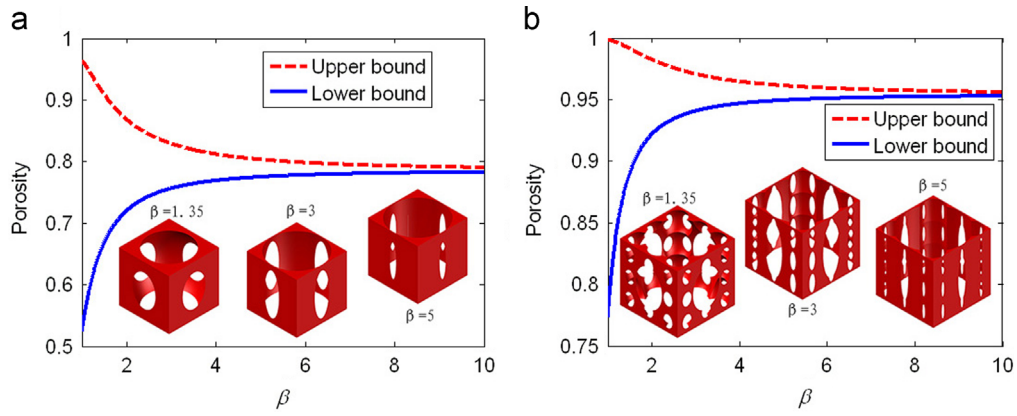
Fig. 2. The porosity range of one-level and two-level structures versus β: (a) one-level unit cell, (b) two-level unit cell.
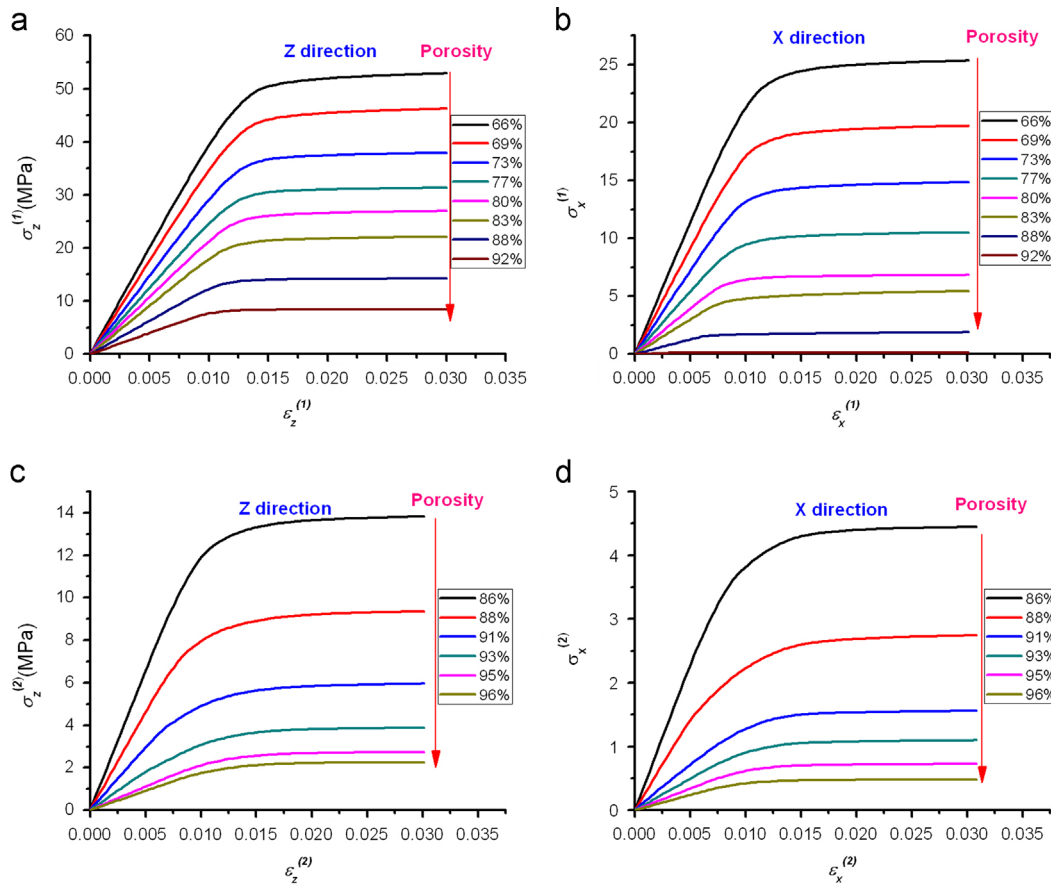
Fig. 3. The structure's strain–stress relationship: (a) one-level scaffold behavior in *Z*-direction, (b) one-level scaffold behavior in *X*-direction (c) two-level scaffold behavior in *Z*-direction, (d) two-level scaffold behavior in *X*-direction.

and two-level scaffolds in *Z*- and *X*-directions, respectively. The mechanical behavior of the scaffold is studied for different β values and porosities.

3.1. Scaffold's strain–stress relationship

In Fig. 3, we illustrate the scaffold's elastic–plastic behavior in different directions for both one-level and two-level models with $\beta = 1.35$. Fig. 3(a) shows the strain–stress relationship of the one-level model with porosity ranging from 66% to 92% in *Z*-direction loading, while Fig. 3(b) shows the strain–stress relationship of the one-level model with the corresponding porosities in *X*-direction loading. It can be observed that the stiffness and strength in *Z*-direction are much higher than that in *X*-direction. It is also seen that the scaffolds

soften as they enter the plastic stage. Fig. 3(c) and (d) show the strain–stress relationship of the two-level model with $\beta = 1.35$. Similar trends are observed as the one-level model. Regardless of β, we observed the stiffness and the strength increase as the porosity decreases, which is also confirmed by the scaffolds based on calcium phosphate [5]. Furthermore, the unhomogenized stress distribution [15], which plays an important role in the material failure, is also observed within the scaffold as reported in the glass–ceramic scaffold model [10].

3.2. Structure's Young's modulus and strength

The structure's Young's modulus and strength are shown in Fig. 4. For the comparison, we have normalized structure's Young's
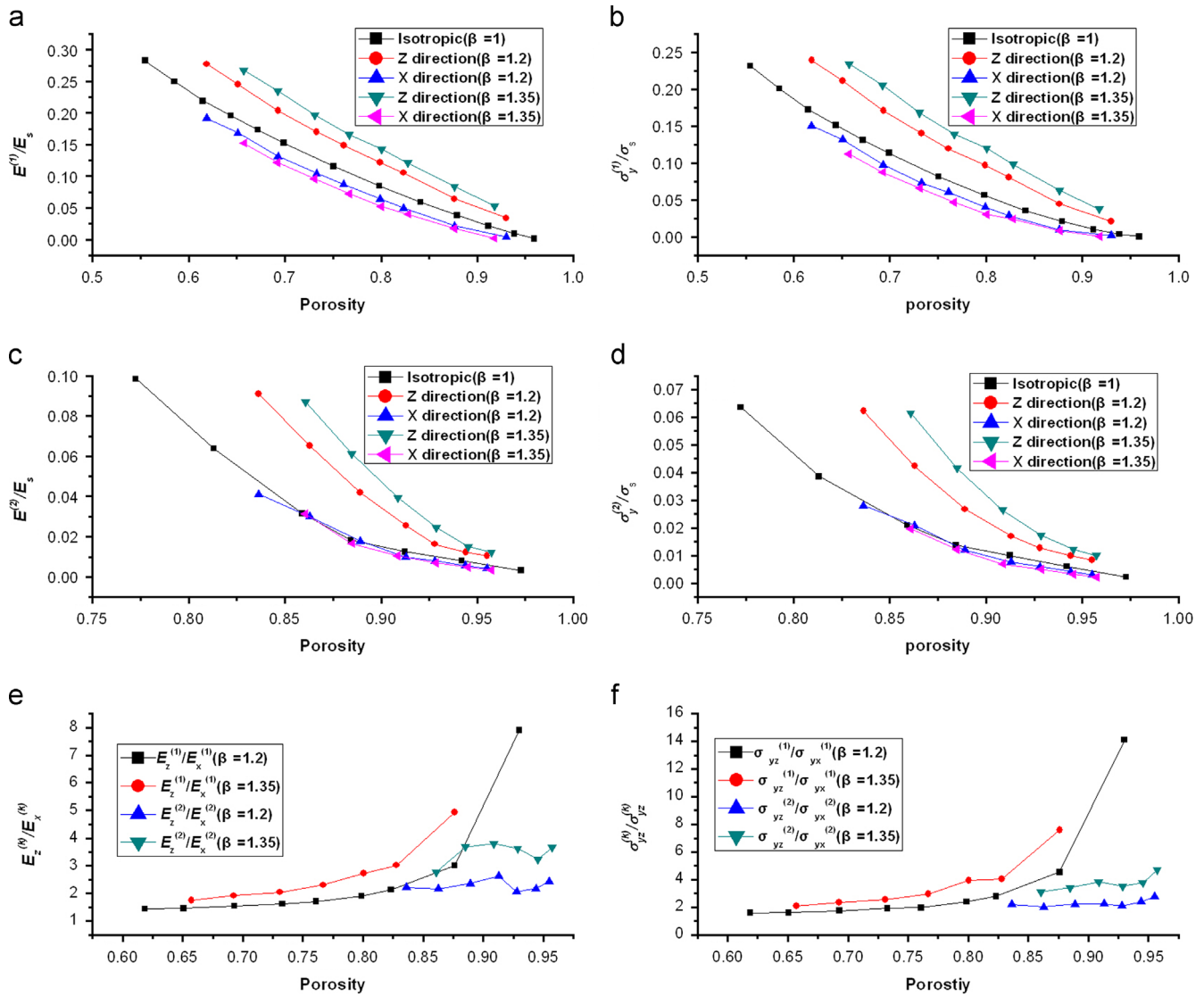
Fig. 4. The normalized structure Young's modulus and strength versus porosity with different β: (a) one-level structure's Young's modulus, (b) one-level structure's strength (c) two-level structure's Young's modulus, (d) two-level structure's strength, (e) mechanical anisotropy ratio of structure's Young's modulus, (f) mechanical anisotropy ratio of structure's strength.

modulus and strength with the Young's modulus and strength of cortical bone, namely $E^{(k)}/E_s$ and $\sigma_y^{(k)}/\sigma_s$ for the one-level and two-level model. It is seen from Fig. 4(a and c) that when $\beta=1$, the one-level and two-level structure's Young's modulus has no difference between Z-direction and X-direction, since the geometry is isotropic in this case. However, as β increases, the structure's Young's modulus exhibits a big difference in Z-direction and X-direction, as seen in Fig. 4(a and c). In particular, when β is 1.35, the ratio $E_Z^{(1)}/E_X^{(1)}$ for one-level scaffold is in the range of 1.76 to 4.93 as the porosity varies from 66% to 88%, while when β is 1.20, the ratio $E_Z^{(1)}/E_X^{(1)}$ for one-level is in the range of 1.46 to 7.91 as the porosity varies from 65% to 93%, as shown in Fig. 4(e). As for the two-level scaffold, when β is 1.35, the ratio $E_Z^{(2)}/E_X^{(2)}$ is in the range of 2.77 to 3.67 as the porosity varies from 86% to 96%, while β is 1.20, the ratio $E_Z^{(2)}/E_X^{(2)}$ is in the range from 2.22 to 2.44 as the porosity varies from 84% to 96%, as seen in Fig. 4(e). The same trend has been observed for the normalized strength of the one-level and two-level models in Fig. 4(b, d and f). Thus, we can see that mechanical anisotropy is affected by the parameter β, where a larger β leads to a higher mechanical anisotropy. The modulus of bone parallel to the longitudinal axis is about 1–5 times larger than that normal to the bone axis [20], which can be easily

implemented by controlling β in our model. It is also noted that for a fixed value of parameter β, higher porosity intensifies mechanical anisotropy in one-level scaffold but its effect on two-level scaffold is not significant, as demonstrated in Fig. 4(e and f). Furthermore, Fig. 4(a) and (b) show a quasi-linear dependence of structure's stiffness and strength on porosity for one-level scaffold, which can be confirmed by the micromechanical approaches [9,19,21], while this dependence is not so clear for two-level scaffold.

4. Conclusions

The stress–strain relationship of a porous anisotropic scaffold with hierarchy is parametrically studied for different β values and porosities. It has been found that mechanical anisotropy depends on the parameter β, where a larger β leads to higher mechanical anisotropy. The proposed scaffold matches the bone's anisotropic behavior and the structural hierarchy. The scaffold's structure is simple and can be achieved easily in manufacturing with controllable porosity and anisotropy. Thus, the scaffold is a promising candidate for bone regeneration.

Acknowledgements

References

[1] Hollister SJ. Scaffold design and manufacturing: from concept to clinic. Adv Mater 2009;21:3330–42.

[2] Zimmermann EA, Schaible E, Bale H, Barth HD, Tang SY, Reichert P, et al. Age-related changes in the plasticity and toughness of human cortical bone at multiple length scales. Proc Nat Acad Sci USA 2011;108:14416–21.

[3] Jones JR, Lee PD, Hench LL. Hierarchical porous materials for tissue engineering. Philos Trans R Soc, Ser A 2006;364:263–81.

[4] Hutmacher DW, Schantz JT, Lam CXF, Tan KC, Lim TC. State of the art and future directions of scaffold-based bone engineering from a biomaterials perspective. J Tissue Eng Regen Med 2007;1:245–60.

[5] Lacroix D, Chateau A, Ginebra M-P, Planell JA. Micro-finite element models of bone tissue-engineering scaffolds. Biomaterials 2006;27:5326–34.

[6] Kabel J, Van Rietbergen B, Odgaard A, Huiskes R. Constitutive relationships of fabric, density, and elastic properties in cancellous bone architecture. Bone 1999;25:481–6.

[7] Malandrino A, Fritsch A, Lahayne O, Kropik K, Redl H, Noailly J, et al. Anisotropic tissue elasticity in human lumbar vertebra, by means of a coupled ultrasound-micromechanics approach. Mater Lett 2012;78:154–8.

[8] Bertrand E, Hellmich C. Multiscale elasticity of tissue engineering scaffolds with tissue-engineered bone: a continuum micromechanics approach. J Eng Mech-ASCE 2009;135:395–412.

[9] Fritsch A, Dormieux L, Hellmich C, Sanahuja J. Mechanical behavior of hydroxyapatite biomaterials: an experimentally validated micromechanical model for elasticity and strength. J Biomed Mater Res Part A. 2009;88:149–61.

[10] Scheiner S, Sinibaldi R, Pichler B, Komlev V, Renghini C, Vitale-Brovarone C, et al. Micromechanics of bone tissue-engineering scaffolds, based on resolution error-cleared computer tomography. Biomaterials 2009;30:2411–9.

[11] Dejaco A, Komlev VS, Jaroszewicz J, Swieszkowski W, Hellmich C. Micro CT-based multiscale elasticity of double-porous (pre-cracked) hydroxyapatite granules for regenerative medicine. J Biomech 2012;45:1068–75.

[12] Lacroix D, Planell JA, Prendergast PJ. Computer-aided design and finite-element modelling of biomaterial scaffolds for bone tissue engineering. Philos Trans R Soc, Ser A 2009;367:1993–2009.

[13] Misra A, Parthasarathy R, Singh V, Spencer P. Micro-poromechanics model of fluid-saturated chemically active fibrous media. ZAMM-J Appl Math Mech/Z Angew Math Mech 2013.

[14] Chen Q, Huang S. Mechanical properties of a porous bioscaffold with hierarchy. Mater Lett 2013;95:89–92.

[15] Huang S, Li Z, Chen Z, Chen Q, Pugno N. Study on the elastic–plastic behavior of a porous hierarchical bioscaffold used for bone regeneration. Mater Lett 2013.

[16] Erol-Taygun M, Zheng K, Boccaccini AR. Nanoscale bioactive glasses in medical applications. Int J Appl Glass Sci 2013;4:136–48.

[17] Johnson T, Socrate S, Boyce M. A viscoelastic, viscoplastic model of cortical bone valid at low and high strain rates. Acta Biomater 2010;6:4073–80.

[18] Niebur GL, Feldstein MJ, Yuen JC, Chen TJ, Keaveny TM. High-resolution finite element models with tissue strength asymmetry accurately predict failure of trabecular bone. J Biomech 2000;33:1575–83.

[19] Fritsch A, Hellmich C, Dormieux L. Ductile sliding between mineral crystals followed by rupture of collagen crosslinks: experimentally supported micromechanical explanation of bone strength. J Theor Biol 2009;260:230–52.

[20] Mow VC, Huiskers R. Basic orthopaedic biomechanics and mechano-biology. Lippincott Williams & Wilkins; 2005.

[21] Hellmich C, Ulm F-J, Dormieux L. Can the diverse elastic properties of trabecular and cortical bone be attributed to only a few tissue-independent phase properties and their interactions? Biomech Model Mechanobiol 2004;2:219–38.